Journal of Electroceramics, 15, 45–56, 2005

Sinterability, Mechanical, Microstructural, and Electrical Properties of Gadolinium-Doped Ceria Electrolyte for Low-Temperature Solid Oxide Fuel Cells

KONDAKINDI RAJENDER REDDY[1] & KUNAL KARAN[1,2,*]

[1]*Fuel Cell Research Centre and* [2]*Department of Chemical Engineering, Queen's University, Kingston, Ontario, Canada K7L 3N6*

Submitted June 30, 2004; Revised January 11, 2005; Accepted March 22, 2005

Abstract. In this study, we report key functional properties of gadolinium-doped ceria ($Gd_{0.1}Ce_{0.9}O_{1.95}$, GDC) sintered at low temperatures as well as single-cell electrochemical performance of a single-cell prepared there of. GDC solid solutions were sintered at various temperatures ranging 1100–1400°C and characterized by X-ray diffraction (XRD), scanning electron microscopy (SEM), density measurements, mechanical strength tests and electrical conductivity measurements. The dry-pressed GDC disc sample sintered at 1100°C was found to have 96% of the theoretical density and higher sintering temperatures led to higher densities. SEM micrographs of the fracture and plan surfaces of the sintered discs established the absence of any open pores. The sample sintered at 1100°C exhibited high electrical conductivity of 0.027 S/cm at 650°C. The mechanical strength of the sintered samples was determined to be in the range of 150–175 MPa. Greater than 96% of theoretical density, good mechanical strength, and high electrical conductivity of GDC disc samples sintered at 1100°C established the viability of low-temperature processing of GDC for its use as an SOFC electrolyte. Accordingly, a single-cell was prepared by co-sintering of GDC electrolyte and LSCF-GDC cathode at 1100°C and subsequent firing of CuO-GDC anode at 900°C. The electrochemical performance of the cell was evaluated in H_2 fuel at 650°C.

Keywords: GDC electrolyte, density, mechanical strength, co-sintering, electrical conductivity, performance

Introduction

Fuel cells are considered to be clean and efficient energy conversion devices. Among the various types of fuel cells, solid oxide fuel cells (SOFCs) offer advantages of higher overall efficiency and fuel flexibility [1]. Conventional SOFCs are based on yttria-stabilized zirconia (YSZ) electrolyte, which constraints the operating temperature to 800–1000°C due primarily to poor ionic conductivity of YSZ at lower temperatures. Unfortunately, high-temperature operation leads to serious design and long-term materials stability problems. As well, expensive high-temperature materials are often required for interconnects and balance-of-the-plant components. High material cost is a major impediment to widespread commercialization of SOFCs [2, 3]. In comparison to higher temperature SOFC based on YSZ-electrolyte, lower-temperature SOFC offer a number of advantages including the use of cheaper materials for interconnects and sealants, lower degradation problems and less thermal mismatch [4].

For lower-temperature (500–700°C) SOFCs, owing to low ionic conductivity of YSZ, alternative electrolyte materials are required. One such class of material is doped-ceria, which was proposed as solid oxide electrolyte in early 1970s [5, 6]. Doped ceria materials possess high ionic conductivity over 500–700°C. However, these materials also exhibit mixed electronic-ionic conductivity, a behavior identified almost three decades back [6, 7]. Reiss [8] presented a generalized mathematical model for treating the electron and ion transports in such mixed conductors. In a subsequent paper, Reiss [9] applied the model to examine the suitability

*To whom all correspondence should be addressed. E-mail: karan@chee.queensu.ca

of using mixed ionic electronic conductor as solid electrolyte. It was concluded that by operating at close to maximum power conditions, the performance loss due to internal electronic currents could be completely suppressed. Later, Reiss et al. [10] and Godickemeier et al. [11] applied the Reiss model [8, 9] for performance characterization of fuel cells and electrodes based on doped-ceria electrolyte.

Among the doped-ceria materials, $Gd_{0.1}Ce_{0.9}O_{1.95}$ (GDC), is considered to be most promising as an electrolyte for SOFCs operating over 500–700°C [12]. In recent years, there has been an increased interest in examining the sinterability of doped-ceria materials as well as assessing its relevant properties for utilization as an SOFC electrolyte [13–15]. For application as a solid electrolyte, it is desirable that the sintered material has a density greater than 95% of the theoretical so as to preclude open porosity and avoid reactant crossover from the anode to the cathode and vice-versa. The sinter density is influenced by a number of factors including sintering temperature and time as well as powder characteristics. El-Halim et al. [16] studied the influence of calcination temperature of powders used to form the green sample on the sinter density. They found that green samples formed with CeO_2 calcined at 600°C yielded the highest density. The maximum sintering density was only 85% theoretical for samples sintered at temperature as high as 1500°C. The relatively low sinter density can be attributed primarily to the large particle size of the powder, which were prepared by conventional methods. Green samples formed by materials of large particle size must be sintered at high temperatures to achieve density high enough to eliminate open porosity [17, 18]. Higher sintering temperature usually produces material of higher density; however, it may also lead to unwanted interfacial reactions during co-sintering of electrolyte and cathode or anode layers [19]. Furthermore, very high-temperature sintering can produce micro-cracks; e.g. due to oxygen liberation as a result of reduction of CeO_2 to Ce_2O_3 [20]. Low-temperature sintering can avoid this problem. The interest in low temperature sintering is also driven by the need to reduce material processing costs.

Recently, it was reported that the GDC can be sintered at temperatures as low as 900°C with the addition of transition metal oxides (TMO), which serves as sintering aids [21, 22]. Although the sintering aids lower the sintering temperature, it can lead to an increased grain boundary resistance to ionic conduction [23] likely due to aggregation of the TMO at the grain boundary as a separate phase. Further, in a study related to sintering behavior of YSZ [24] it was found that grain boundary effect due to segregation of silica was further enhanced in the presence of MnO_2 (a TMO used as a sintering aid). The synergistic effect of MnO_2 and silica was attributed to the formation of a glass phase.

In addition to high sinter density and high ionic conductivity, it is desirable that the electrolyte membrane possesses reasonable mechanical strength. Few studies have reported the mechanical strength of the doped-ceria samples [25–27]. Little information is available on the mechanical strength of the GDC samples sintered at low temperatures.

The goal of this study was to investigate the lowest possible sintering temperature that produced electrolyte membrane of acceptable mechanical integrity, density and electrical conductivity. The requirement of low sintering temperature was driven by the need to allow co-sintering of $La_{0.6}Sr_{0.4}Co_{0.2}Fe_{0.8}O_3$(LSCF)–$Gd_{0.1}Ce_{0.9}O_{1.95}$ (GDC) composite cathode and GDC electrolyte layers.

Experimental

GDC Characterization

GDC powder of crystallite size around 10 nm was obtained from Nextech Materials, Inc., USA. Phase identification of the as-received powder was performed on Philips X'Pert MPD diffractometer with Co Kα radiation in the range of 30–110° 2θ. The diffractogram was analyzed to obtain crystallite size using Scherrer's equation based on the intensity of (111) reflection of GDC. Instrument peak broadening was accounted for in the reported crystallite size.

The density, mechanical strength and electrical conductivity measurements were conducted on sintered GDC disc samples. For preparation of disc samples, the as-received GDC powder was first calcined at 700°C for 7 h and material sieved through 100 mesh were utilized. The disc samples with 13 and 31 mm diameter were prepared by uniaxial dry pressing at 200 MPa. The die set was evacuated during pressing. The applied load was increased in steps of 30 MPa from zero to 200 MPa with a hold time of 15 sec at each step. No binder was added for the preparation of the discs. The green discs were sintered for 5 h at various temperatures over the 1100–1400°C range. A heating rate of 1°C/min and a cooling rate of 5°C/min were applied

to eliminate any thermal stress. Density measurements of GDC ceramic discs were carried out on an AccuPyc 1330 gas pyconometer (Micromeritics, USA). Triplicate density measurements on each disc sample were carried out. The level of porosity was further examined by scanning electron microscopy (SEM) of the fracture and plan surfaces of the sintered GDC disc samples. A JEOL JSM 5800 instrument operated at 10 KeV was used for recording SEM micrographs. Transmission electron micrographs (TEM) of the as-received GDC powder and the sintered GDC samples were recorded on Philips 400 T instrument at 120 KeV. For TEM analysis of the sintered samples, the sintered discs were crushed into powder, ultrasonically dispersed in methanol and then dispersed onto formvar coated copper grids.

The mechanical strength of the sintered GDC discs was characterized in terms of biaxial flexural strength. The biaxial flexural strength was measured according to the ASTM F-394 method. A three-point bend set-up coupled to a computer controlled Instron 4202R machine was utilized. Measurements were carried out on a sintered disc of ∼1 mm thickness and ∼26 mm diameter. For testing, as-sintered discs were used without any surface treatment permissible under F-394 method. Briefly, the experiment involved placing the sintered disc sample on three stainless steel ball supports as shown in Fig. 1, followed by application of a known force at a rate of 0.02 inch/sec perpendicular to the sample plane. The load at fracture was recorded and mechanical strength calculated according to formula specified in the ASTM F-394 procedure.

The electrical conductivity of the sintered discs in air was measured by a 4-probe two-point ac impedance method using a Solartron SI 1260 frequency response analyzer. To ensure a good contact between the platinum wires and the disc, each side of the disc was painted with silver paste after they had been polished and annealed at 700°C for 1 h. Measurements were made from 0.01 Hz to 5 MHz over temperature ranging 150–700°C at an excitation voltage of 50 mV for all temperatures and all frequencies.

Single-cell Preparation: For the preparation of a single-cell, first, a GDC electrolyte membrane was prepared by uniaxial dry pressing of the GDC powder at 200 MPa. Following this, a composite cathode comprising 50 wt% each of $Gd_{0.1}Ce_{0.9}O_{1.95}$ (GDC) and $La_{0.6}Sr_{0.4}Co_{0.2}Fe_{0.8}O_3$ (LSCF) was applied by slurry painting on one side of the electrolyte membrane. The GDC-LSCF cathode slurry was prepared by ball milling of a mixture of GDC, LSCF, binder, solvent and dispersant for 5 h with zirconia balls. The cathode painted GDC electrolyte was co-fired at 1100°C for 5 h with a heating rate of 1°C/min and a cooling rate of 5°C/min. Next, CuO-GDC (69 wt% CuO, Alfa Aesar) anode was slurry painted on the other side of the electrolyte. The anode slurry was prepared by ball milling a mixture of CuO, GDC, solvent, binder and dispersant. The prepared single-cell was subsequently fired at 900°C for 3 h with heating and cooling rates of 3°C/min. The thickness of the electrolyte layer after sintering was ranged from 600 to 750 μm. For the evaluation of single-cell electrochemical performance, Pt mesh and wire were attached to both the electrodes with the Pt paste (A4338A, Engelhard). The cell with an active area of 1 cm^2 was sealed onto the alumina tube with silver paste. The current-voltage characteristics of the cell were measured in the temperature range 600–650°C with humidified H_2 (3 vol% H_2O) as the fuel and air as the oxidant. The cell impedance was measured in the frequency range of 100–0.01 Hz using a Solartron SI 1260 frequency response analyzer in combination with Solartron 1287 electrochemical interface.

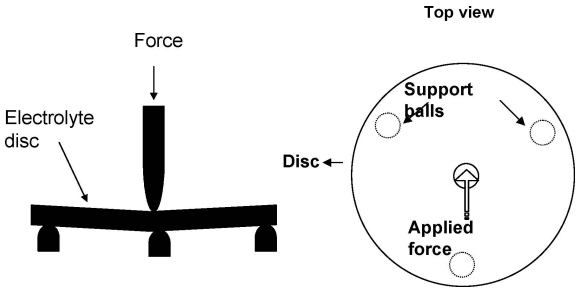

Fig. 1. Schematic diagram of the 3-point bend set-up.

Results and Discussion

GDC Characterization

XRD Analysis: Figure 2 shows the XRD patterns of various GDC disc samples sintered at different temperatures. The as-received powder was essentially amorphous to X-rays. For the GDC powder treated at 700°C, all the reflections corresponding to fluorite structure of ceria were observed (JCPDS: 34-394). The XRD peak broadening in Fig. 2 indicates that the crystallite size of the calcined powder is small. As

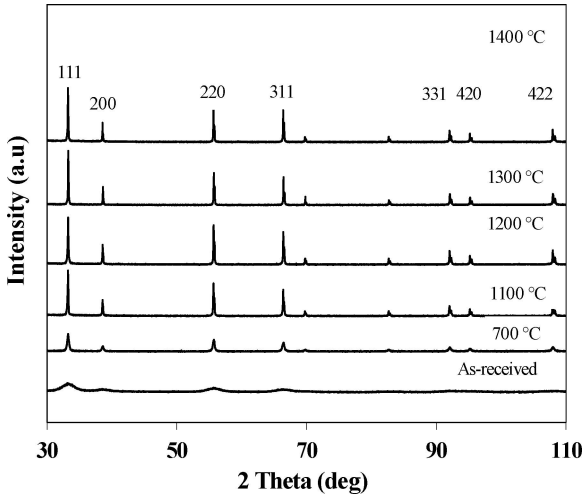

Fig. 2. X-ray diffraction patterns of various $Gd_{0.1}Ce_{0.9}O_{1.95}$ samples.

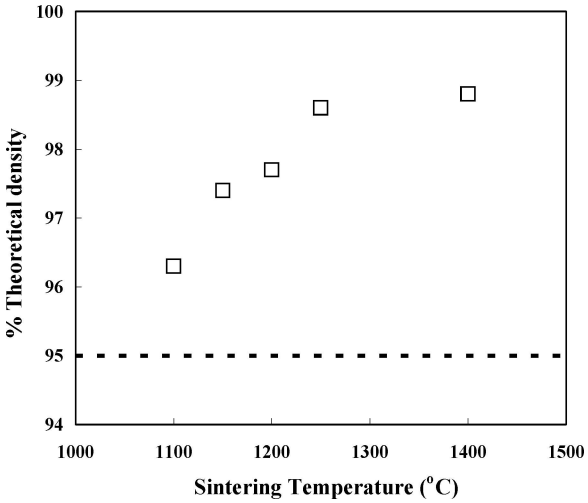

Fig. 3. Density measurements of various $Gd_{0.1}Ce_{0.9}O_{1.95}$ samples.

expected, the peak broadening decreases with an increase in temperature implying an increase in the crystallite size. The intensities of all the reflections increased with an increase in temperature. The crystallite sizes calculated from Scherrer equation are reported as a function of sintering temperature in Table 1.

Density Measurements: The relative densities of the green discs based on measured dimensions were calculated to be in the range of 55–60%. These are comparable to the density reported by Zhang et al. [17] who also prepared green discs by uni-axial pressing to 200 MPa. The density of the sintered discs as a function of sintering temperature is shown in Fig. 3. For the $Gd_xCe_{1-x}O_{2-x/2}$ sample the theoretical density can be calculated using the following equation:

$$d_{\text{th}} = 4/N_A a^3[(1–x)M_{Ce} + xM_{Gd} + (2–0.5x)M_O] \quad (1)$$

where a is the lattice constant of the solid solution at room temperature, which is equal to 0.5422 nm [28], N_A is the Avogadro number and M refers to the atomic weight. For the GDC composition used in the present study x is equal to 0.1, which yields a theoretical density of 7.21 g/cm^3.

In Fig. 3, each data point corresponds to an average of measurements on 3 disc samples. In the figure, the dashed line corresponds to what is generally considered to be an acceptable level of density (>95%) for the use of sintered sample as an impermeable electrolyte membrane in an SOFC. Clearly, the data indicates that the theoretical densities of more than 95% can be achieved by sintering the green discs at temperatures as low as 1100°C. Using similar nano-sized powders, Zhang et al. [17] reported the density of the sample sintered at 1100°C to be around only 85%. However, they obtained greater than 99% of the theoretical for samples sintered at 1250°C. Zhang et al. [17] had also studied the influence of powder pre-calcination temperature on sinter density. They found that powders calcined at 700°C yielded highest sinter density. In the present study, we had pre-calcined the powder at 700°C as well although no attempts were made to optimize the calcination temperature. Finally, it may be useful to add that in the

Table 1. Crystallite size measurements of GDC samples by X-ray diffraction.

S.No.	Sintering temperature (°C)	Crystallite size (nm)
1	As-received	20 (<10)
2	700	99
3	1100	210 (220)
4	1200	230
5	1300	231
6	1400	290 (300)

The values in the brackets are the crystallite sizes estimated from TEM.

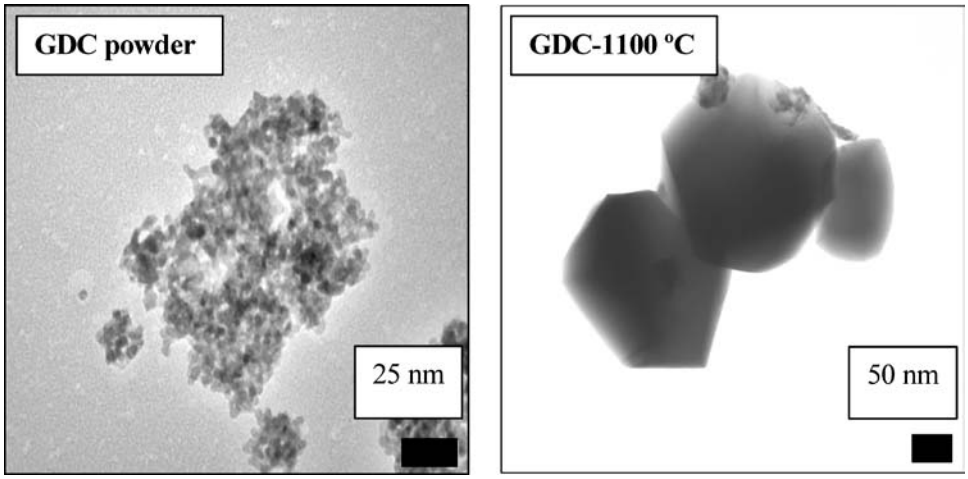

Fig. 4. Transmission electron micrographs of as-received and 1100°C sintered $Gd_{0.1}Ce_{0.9}O_{1.95}$ samples.

present study, relatively high densities were obtained without the addition of any dopants. The high density of the samples is attributed to a combination of at least two factors—(i) high green density resulting from use of GDC powder calcined at 700°C and (ii) small crystallite size, which offers large surface area for solid state diffusion during sintering [29].

Microstructural Analysis: Microstructure of the GDC powders was investigated by means of transmission electron microscopy whereas that of sintered samples by scanning electron microscopy. Figure 4 shows the transmission electron micrographs of the as-received GDC powder and that of GDC disc sintered at 1100°C (TEM was recorded after crushing the disc into powder). From the figure, the crystallite sizes of the as-received and 1100°C sintered sample can be estimated to be <10 nm and ∼220 nm, respectively. These crystallite sizes are in good agreement with the crystallite sizes calculated from X-ray diffraction data. Figure 5 shows the scanning electron micrographs of the fracture surfaces of various GDC samples sintered at different temperatures. Figure 5(a) shows the cross-section of GDC disc sintered at 1100°C. It can be clearly observed in the micrographs that the sample has no cracks or deformation. Further, no open pores are observed, although some closed pores are clearly visible. The scanning electron micrographs of the plan surface of the sintered samples are shown in Fig. 6. The figure reveals the grain microstructure as a function of sintering temperature. The average grain size, estimated from image analyses of 2 micrographs, increased from ∼0.25 μm to ∼2 μm as the sintering temperature increased from 1100 to 1400°C.

Mechanical Strength: The mechanical strength of disc samples sintered at various temperatures was evaluated in terms of flexural strength. The data is presented in Table 2. The reported mechanical strength data are a mean of measurements on 5 samples for each sintering temperature. The data indicates that the mechanical strength decreases with an increase in sintering temperature over the range 1100–1300°C. The low mechanical strength at high sintering temperatures is likely due to the increased stress concentration in large grains as the grain size increased when the sintering temperature increased from 1100 to 1300°C. Bellon et al. [27] have determined flexural strengths for GDC rods and tubes. They reported flexural strength as high as 220 MPa for samples sintered at 1600°C. Sameshina et al. [25] have reported flexural strength of samaria-doped ceria, determined via 4-point flexural method, to be in the order of 50–80 MPa for samples sintered at 1600°C. Our flexural strength data for GDC sintered over 1100–1400°C range from 150 to 170 MPa. These values are higher

Table 2. Flexural strength measurements of various GDC samples.

S.No.	Sintering temperature (°C)	Average grain size (μm)	Flexural strength (MPa)
1	1100	0.25	175 ±10
2	1200	0.80	155 ±10
3	1300	1.10	150 ±10

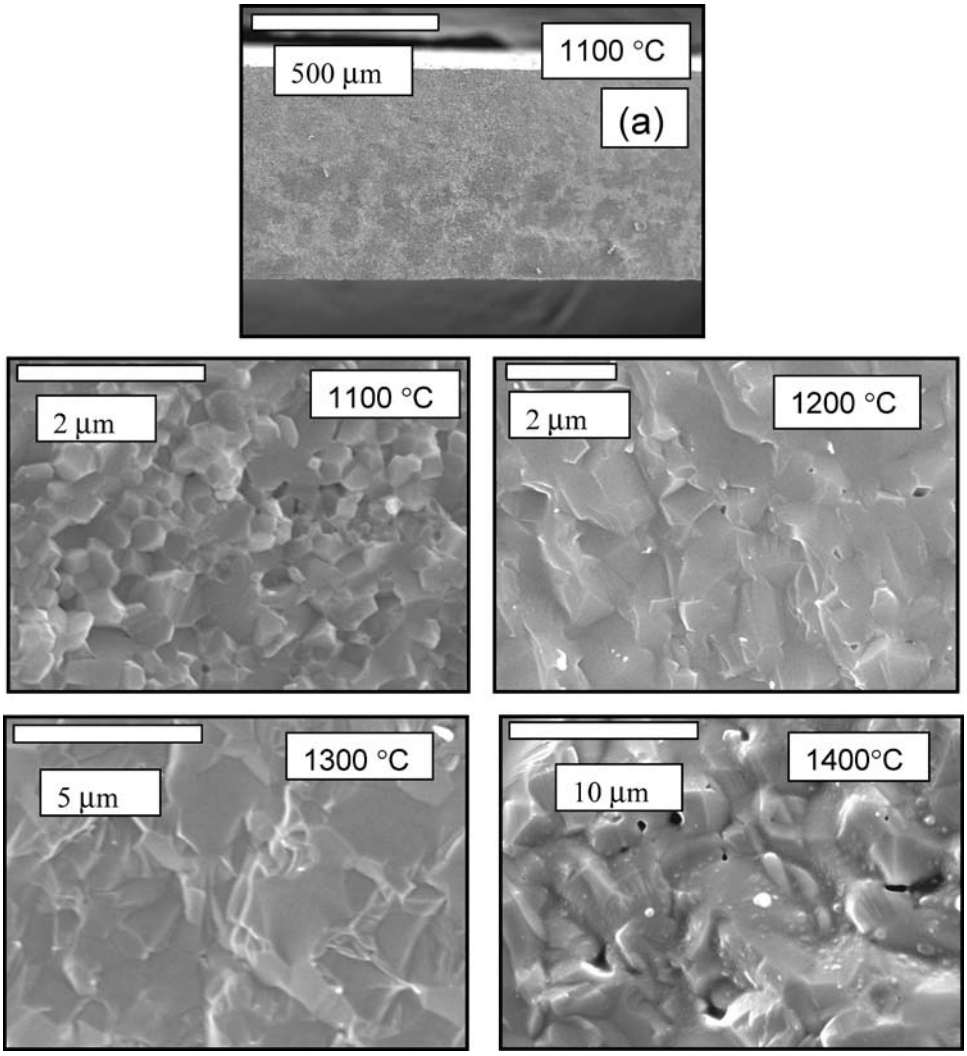

Fig. 5. Scanning electron micrographs of fracture surfaces of $Gd_{0.1}Ce_{0.9}O_{1.95}$ samples.

than those reported by Sameshina [25] but lower than those determined by Bellon et al. [27]. In comparison, the mechanical strength values for sintered YSZ samples have been reported to be higher than 300 MPa [30, 31].

Electrical Conductivity: The electrical conductivity of the sintered samples was determined by impedance spectroscopy measurements. Impedance spectroscopy helps to resolve the grain and grain-boundary conduction as well as the electrode kinetic processes. The response of these processes manifests as semi-circles in a Nyquist plot [32]. Figure 7 shows the impedance spectra of a GDC disc, sintered at 1100°C, in air at various test temperatures. At the test temperature of 150°C, Fig. 7 shows three distinct semicircles corresponding to the responses of grain conduction (80 kHz), grain boundary conduction (160 Hz) and electrode processes. As expected, with an increase in temperature the resistances associated with each of the three processes decreased drastically. The response of the grain boundary conduction process was observed at 150 and 200°C. However, owing to short relaxation time for the grain resistance, the semicircle corresponding to grain resistance is not observed at 400°C and higher temperatures.

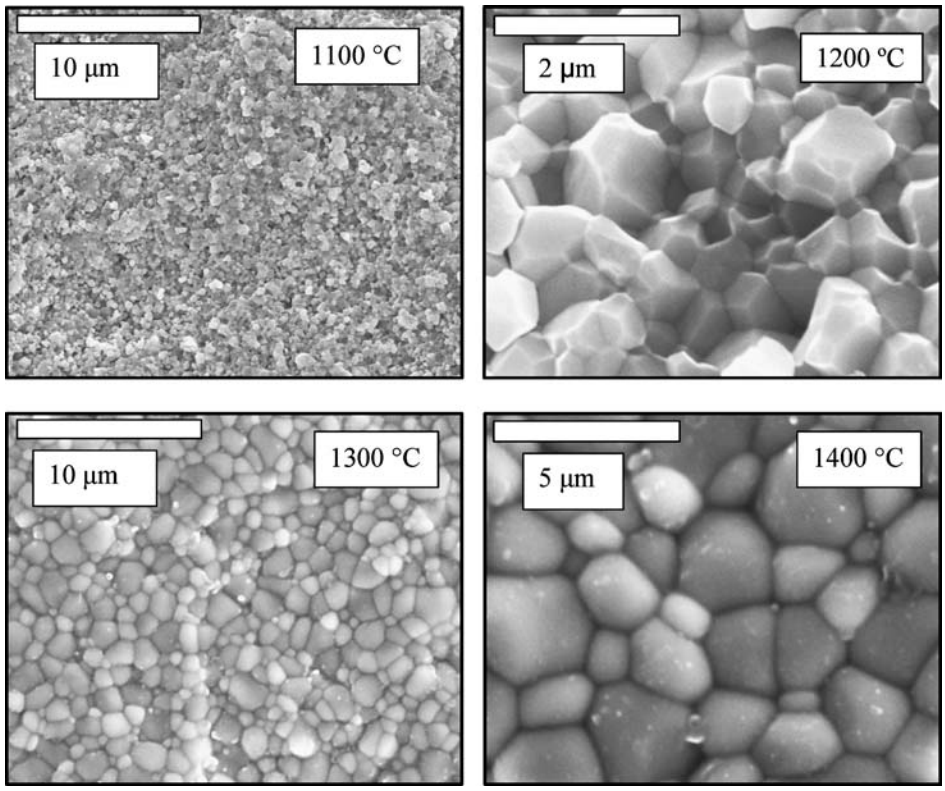

Fig. 6. Scanning electron micrographs of plan surfaces of $Gd_{0.1}Ce_{0.9}O_{1.95}$ samples.

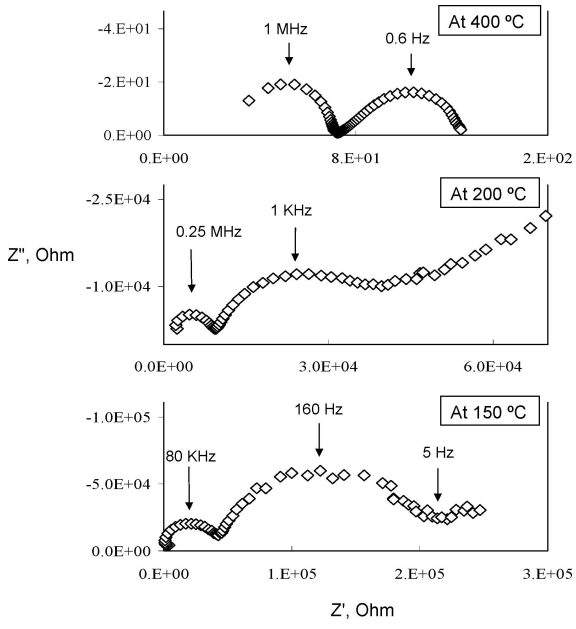

Fig. 7. Impedance spectra of $Gd_{0.1}Ce_{0.9}O_{1.95}$ sample measured in air sintered at 1100°C.

Each semi-circular response on the Nyquist plot was fitted with a simple circuit comprising of a resistance and capacitance in parallel using the ZView® software. The capacitance of the grain at 150°C was accordingly estimated to be 5.8×10^{-11} farads, which compares well with 10^{-10} farads reported in another study [33].

Figure 8 shows the plots of the conductivities of sintered GDC samples in air as a function of inverse of test temperature. The data for the samples sintered at 1100°C are compared with those for samples sintered at 1200 and 1400°C. From the data presented in Fig. 8, it can be concluded that the electrical conductivity of samples sintered at 1100, 1200 and 1400°C are comparable within the measurement errors. GDC conductivities reported in this work are higher than those reported by Zhou et al. [33], Dikmen et al. [34], Zhang et al. [35] but lower than those reported by Steele [12].

The total electrical conductivity can be described in terms of an Arrhenius-type relationship, wherein a plot of ln (σT) versus $1/T$ yields a straight line with slope $-Ea/k$, provided the activation energy, Ea,

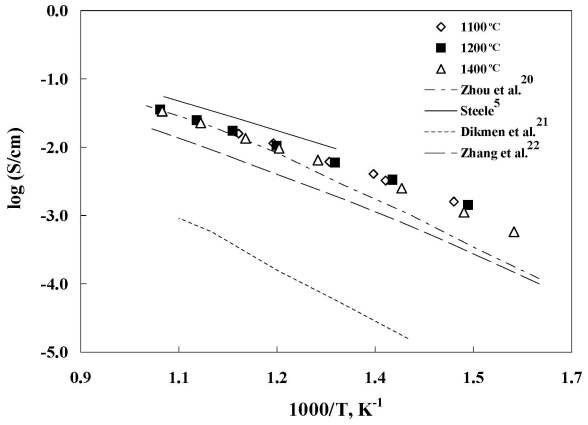

Fig. 8. Temperature dependence of electrical conductivity of various $Gd_{0.1}Ce_{0.9}O_{1.95}$ samples in air.

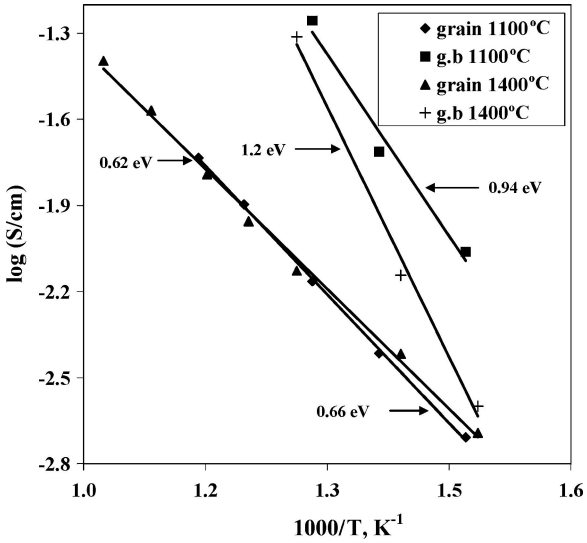

Fig. 9. Dependence of grain and grain boundary conductivities of $Gd_{0.1}Ce_{0.9}O_{1.95}$ samples as a function of temperature.

is independent of temperature. For GDC conductivity, the plot of $\ln(\sigma T)$ versus $1/T$ usually exhibits two distinct slopes each at temperatures greater than and lower than a critical temperature, which has been reported be as low as 400°C [12] and as high as 583°C [28]. This temperature corresponds to the dissociation of dopant-oxygen vacancy complexes [33]. Our data in Fig. 8 corresponds at temperatures greater than 400°C and expectedly demonstrates a linear relationship without a curvature as reported elsewhere [36, 37]. The activation energies of the total conductivity for the samples sintered at 1100 and 1400°C were estimated to be 0.66 and 0.71 eV, respectively. These activation energies are lower than those reported in the literature [34, 35, 38]. According to Steele [12], the activation energy for the conductivity of pure GDC is around 0.64 eV. However, low conductivity impurities segregated in the grain boundary region can lead to significantly higher overall activation energy in the order of 1 eV. Because the GDC powder used in this study exhibited activation energies around 0.68 eV, it is safe to state that the sample is relatively pure. Nextech Materials, Inc., the suppliers of the GDC powder state that the amount of SiO_2 present in the GDC sample, as determined by X-ray fluorescence, is <10 ppm [39].

The grain and grain boundary (g.b) conductivities of GDC samples sintered at 1100 and 1400°C are presented in Fig. 9. In the present study, the grain boundary resistance disappeared at temperatures above 500°C. The activation energies for the grain conductivity of the samples sintered at 1100 and 1400°C are 0.66 and 0.62 eV, respectively, whereas the activation energies for the grain boundary conductivity are 0.94 and 1.2 eV, respectively. Samples sintered at 1100 and 1400°C have average grain sizes of 0.25 and 2 microns, respectively. The activation energies of the grain conductivity for these two samples are close to each other regardless of the grain size as reported elsewhere [33].

In a majority of previous literature, the low grain boundary conductivity has been attributed to the segregation of silica impurity at grain boundary [12, 40, 41]. More recently, Kim and Maier [42] have attempted to explain the grain boundary activation energy in terms of space-charge potential distributions. They especially emphasized the importance of this phenomenon in nano-sized particles. They estimated the grain boundary activation energy of GDC due to space-charge distribution to be in the order of 1.5 eV. Based on the measured activation energy, it appears that the grain boundary effect for our sample is a result of the presence of very small concentration of silica and not due to the space-charge distribution. It must be re-emphasized that for the level of silica present in the GDC samples used in this study, the grain boundary effect is prominent only at low temperatures and has minimal impact on the overall conductivity at temperatures of interest (500–700°C) for SOFC operation.

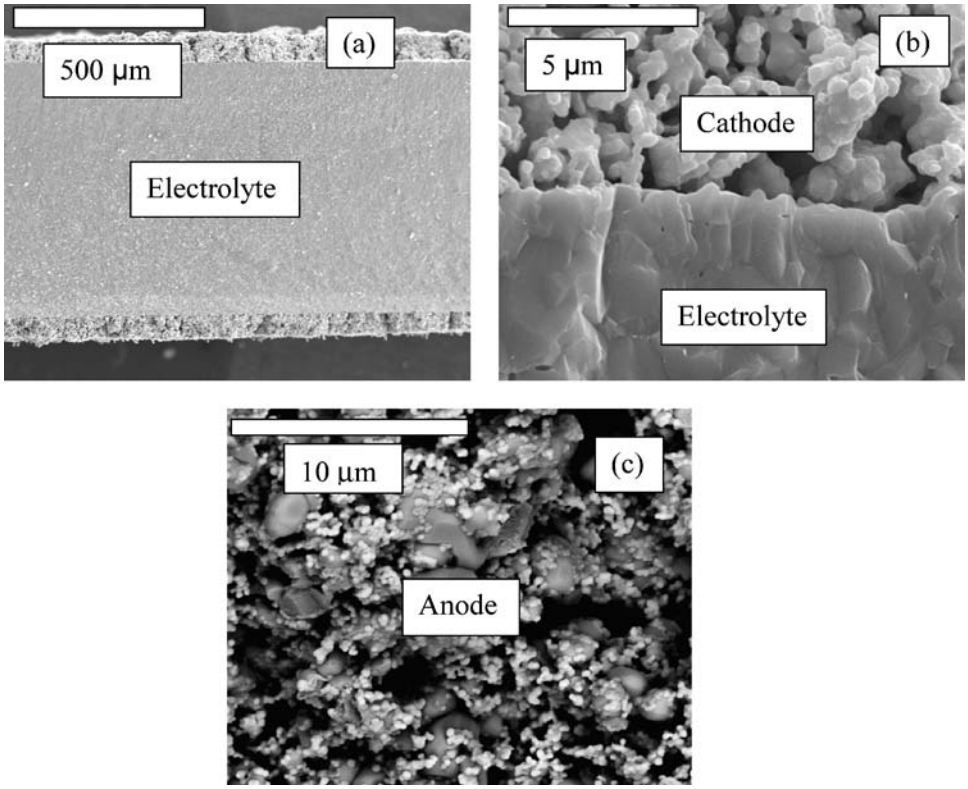

Fig. 10. SEM micrographs of CuO-GDC//GDC//GDC-LSCF single cell.

Performance of Single-Cell SOFC Fabricated by Low-Temperature Processing

GDC sample sintered at 1100°C has all the key functional properties for the use as an electrolyte for low-temperature applications—high density, high electrical conductivity and high mechanical strength. To exploit high sinterability of GDC at 1100°C, a single cell was prepared by co-firing of the cathode and electrolyte at 1100°C. The electrochemical performance of the cell was evaluated to study the losses associated with the electrodes and electrolyte. To characterize the porosity and interfacial adhesion of the electrolyte and electrodes, SEM micrographs of the CuO-GDC//GDC//GDC-LSCF cell were recorded and are presented in Fig. 10. The SEM micrograph of a complete single cell, with electrolyte and electrodes, is shown in Fig. 10(a). Figure 10(b) shows the electrolyte-cathode interface and it may be observed that the cathode layer is porous. Figure 10(c) shows the high resolution back-scattered SEM micrograph of the CuO-GDC anode. From the figure, it may be observed that there is a uniform distribution of CuO (dark and large particles, which was confirmed by Energy Dispersive X-Ray Spectroscopy (EDXS)) and GDC particles (small and bright particles, which was confirmed by EDXS). Although the distribution is uniform, it is clear that the CuO particles are significantly larger than the GDC particles. The large difference in particle size distribution is expected to result in a smaller number of percolating triple-phase boundary regions and, thereby, resulting in higher electrode polarization. The thickness of the anode and cathode from the micrographs were estimated to be approximately 60 and 70 μm, respectively. For the evaluation of electrochemical performance of the fabricated single-cell SOFC, humidified H_2 (3% H_2O balance H_2) and air were used as fuel and oxidant, respectively. The impedance spectra of the single cell were measured under open circuit conditions and are shown in Fig. 11. The serial or ohmic resistance (Rs, primarily due to electrolyte) for the cell is 3.1 and 7.5 Ohm·cm^2 at 650 and 600°C, respectively. The

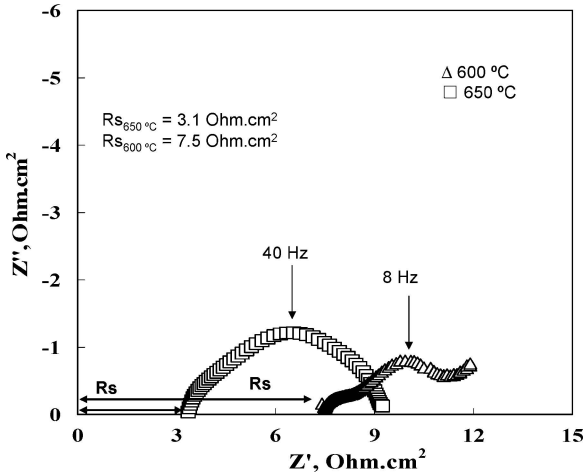

Fig. 11. Typical impedance spectra of the CuO-GDC (H_2) //GDC//GDC-LSCF (air) single cell measured under open circuit conditions (R_s = serial resistance).

current-potential characteristics of the cell, measured at 650°C, are shown in Fig. 12. The open circuit voltage (OCV) was measured to be 0.935 V. This OCV is lower than the theoretical voltage calculated using Nernst equation and is attributed to mixed ionic-electronic conductivity (MIEC) of GDC sample at high temperatures because of reduction of Ce^{4+} to Ce^{3+} in the reducing atmosphere. Thus, even at open circuit conditions, both ionic and electronic current flows internally although the net current is zero. This phenomenon has

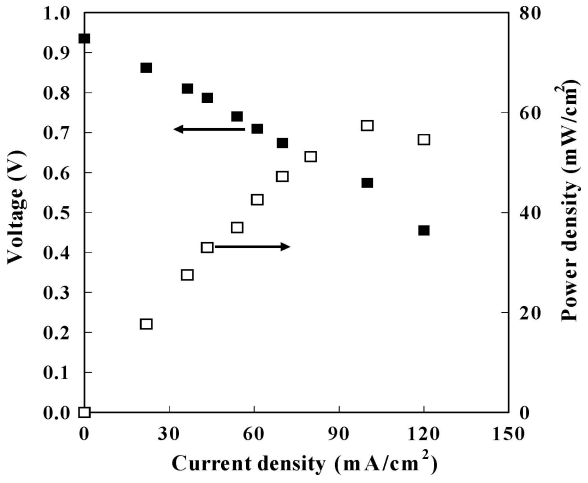

Fig. 12. Current-voltage characteristics of the CuO-GDC (H_2)// GDC//GDC-LSCF (air) single cell measured at 650°C.

been observed by other researchers as well as mathematically modeled [8–12, 43]. We calculated the theoretical OCV for GDC according to method reported by Sahibzada et al. [43]:

$$V_{th} = V_n - j_i(R_a + R_c) \tag{2}$$

where, V_n is the Nernst potential, j_i is the ionic leakage current at open circuit conditions and R_a and R_c are the equivalent anodic and cathode polarization resistances. Under OCV conditions, the electronic leakage current is equal to the ionic leakage current, i.e. $j_e = j_i$. To calculate the leakage current the following equation is solved:

$$j_e = \frac{\sigma_i}{L} \times \left[\frac{P(-)}{\exp\left(-\frac{4RT}{F(V_{th}+j_i R_c)}\right)}\right]^{1/4} \times j_i R_i \frac{\exp\left(\frac{F}{RT}(V_n - j_i(R_i + R_a + R_c))\right) - 1}{1 - \exp\left(-\frac{F(j_i R_i)}{RT}\right)} \tag{3}$$

where, σ_i is the ionic conductivity of GDC electrolyte, L is the electrolyte thickness, R_i is the total ionic resistivity, $P(-)$ is the partial pressure at which ionic and electronic conductivities are equal, F is Faraday's constant, R is universal gas constant and T is temperature. The following correlations for total conductivity of GDC as a function of temperature for our sample and that for $P(-)$ reported by Steele [12] were employed:

$$\log[\sigma_i] = -\frac{3042}{T} + 1.6793 \tag{4}$$

$$\log[P(-)] = -\frac{3.697 \times 10^4}{T} + 18 \tag{5}$$

The ionic resistance, R_i, was approximated as the serial resistance (R_s = 3.0 ohms-cm^2 at 650°C) determined from impedance measurements at open circuit conditions. The total electrode polarization ($R_a + R_c$ = 6.2 ohms-cm^2 650°C) was also estimated from impedance measurement at open circuit conditions. As a first approximation, the total electrode polarization was assumed to be equally contributed by anode and cathode processes, i.e. $R_a = R_c = 3.1$ ohms-cm^2. The assumption of equal electrode resistance is not necessarily justifiable given the fact that polarization effects associated with oxygen reduction reaction at cathode usually dominates. Further, it must be clarified that the

total electrode resistance ($R_a + R_c$) is a lumped parameter containing both charge-transfer and concentration polarizations. Furthermore, as indicated in references [10, 11] the electrode resistances will vary as a non-linear function of the external current. As such, the total electrode resistance value determined from impedance spectroscopy is valid only for open-circuit conditions.

The Nernst voltage was calculated to be 1.10 V from the known partial pressure of oxygen in air on the cathode side and calculated oxygen partial pressure on the anode side for 97 vol% H_2-3 vol% H_2O mixture (P_{O_2}= 6.23×10^{-26} bars). Using an electrolyte thickness of 650 micron, the theoretical OCV was calculated using Eq. (2) to be 0.946 V at 650°C, which is slightly higher than the measured OCV of 0.935 V. The difference between estimated and calculated OCVs is relatively small and can be attributed to a number of factors including possible hydrogen cross-over as well as accuracy of $P(-)$ and ionic conductivity values. Nonetheless, this simplified analysis allows us to generate a reasonable estimate of the OCV for fuel cell based on mixed conducting GDC electrolyte. It is useful to add that owing to the form of equation, the calculated OCV is insensitive to how the total electrode resistance is split into R_a and R_c. For instance, assuming $R_a = 0$ and $R_c = 6.2$ ohm-cm^2, the OCV is calculated to be 0.946 V.

Finally, it is recognized that the maximum power density of 60 mW/cm^2 obtained at 650°C is fairly low. Further improvements in the anode and cathode microstructure design as well as a reduction in the electrolyte thickness are currently underway to increase the current and power densities.

Conclusions

Nano-sized gadolinium-doped ceria powder was successfully sintered to high relative density (>96%) at a sintering temperature as low as 1100°C. The electrical conductivity of the sample sintered at 1100°C was also determined to be reasonably high in comparison to previously reported data in the literature. Furthermore, the mechanical strength of the GDC disc sample sintered at 1100°C was determined to be 175 MPa, which is reasonably high. The single cells prepared by low-temperature co-firing of GDC electrolyte and cathode layers were tested successfully at 650°C. The measured maximum power density was low (60 mW/cm^2) implying that further modifications in the anode and cathode microstructure and the electrolyte thickness are essential to improve the performance of the cell.

Acknowledgments

The authors acknowledge Centre for Automotive Materials and Manufacturing (CAMM) and Natural Sciences and Engineering Research Council (NSERC), Canada for the financial support. The authors are also thankful to Alcan International, Kingston for providing access to scanning electron microscope and Instron machine.

References

1. M. Sahibzada, B.C.H. Steele, K. Zheng, R.A. Rudkin, and I.S. Metcalfe, *Catal. Today*, **38**, 459 (1997).
2. M. Dokiya, *Solid State Ionics,* **152/153**, 383 (2003).
3. J. Thissjen et al., Arthur D. Little Report, #71316 (2000).
4. N.Q. Minh, *J. Amer. Ceram. Soc.,* **76**, 563 (1993).
5. T.H. Etsell and S.N. Flengas, *Chem. Rev.*, **70**, 339 (1970).
6. H.L. Tuller and A.S. Nowick, *J. Electrochem. Soc.*, **122**, 255 (1975).
7. B.C.H. Steele and J.M. Floyd, *Proc. Brit. Ceramic Society*, **19**, 55 (1971).
8. I. Reiss, *J. Electrochem. Soc.*, **128**, 2077 (1981).
9. I. Reiss, *J. Phys. Chem. Solids*, **47**, 129 (1986).
10. I. Reiss, *Solid State Ionics*, **51**, 127 (1992).
11. I. Reiss, M. Godickemeier, and L.J. Gauckler, *Solid State Ionics*, **90**, 91 (1996).
12. M. Godickemeier, K.Sasaki, L.J. Gauckler, and I. Reiss. *J. Electrochem Soc.*, **144** (5), 1635 (1997).
13. B.C.H. Steele, *Solid State Ionics,* **129**, 95 (2000).
14. J. Ma, T.S. Zhang, L.B. Kong, P. Hing, and S.H. Chan, *J. Power Sources,* **132**, 71 (2004).
15. T.S. Zhang, J. Ma, L.B. Kong, P. Hing, Y.J. Leng, S.H. Chan, and J.A. Kilner, *J. Power Sources,* **124**, 26 (2003).
16. J.-G. Li, T. Ikegami, Y. Wang, and T. Mori, *J. Amer. Ceram. Soc.*, **86**, 915 (2003).
17. A.S.A. El-Halim, N.M. Adelmonem, N.A. Afify, and G.A. El-Hamid, *Powder Met. Int.*, **21**, 29 (1989).
18. T.S. Zhang, J. Ma, Y.J. Leng, S.H. Chan, P. Hing, and J.A. Kilner, *Solid State Ionics*, **168**, 187 (2004).
19. R.S. Torrens, N.M. Sammes and G.A. Tompsett, *Solid State Ionics,***111**, 9 (1998).
20. A. Tsoga, A. Naoumidis and D. Stover, *Solid State Ionics*, **135**, 403 (2000).
21. C.M. Kleinlogel, Ph.D thesis, Swiss Federal Institute of Technology, Zurich, 1999.
22. C. Kleinlogel and L.J. Gauckler, *Solid State Ionics*, **135**, 567 (2000).
23. C. Kleinlogel and L.J. Gauckler, *Adv. Mater.*, **13**, 1081 (2001).

24. T.S. Zhang, L.B. Kong, Z.Q. Zeng, H.T. Huang, P. Hing, Z.T. Xia, and J.A. Kilner, *J. Solid State Electrochem.*, **7**, 348 (2003).
25. C.C. Appel and N. Bonanos, *J. Eur. Ceram. Soc.*, **19**, 847 (1999).
26. S. Sameshima, T. Ichikawa, M. Kawaminami, and Y. Hirata, *Mat. Chem. Phys.*, **61**, 31 (1999).
27. T.S. Zhang, J. Ma, L.B. Kong, P. Hing, and J.A. Kilner, *Solid State Ionics*, **167**, 191 (2004).
28. O. Bellon, N.M. Sammes, and J. Staniforth, *J. Power Sources*, **75**, 116 (1998).
29. K. Huang, M. Feng, and J.B. Goodenough, *J. Amer. Ceram. Soc.*, **81**, 357 (1998).
30. S. Nakane, T. Tachi, M. Yoshinaka, K. Hirota, and O. Yamaguchi, *J. Amer. Ceram. Soc.*, **80**, 3221 (1997).
31. J.W. Adams, R. Ruh, and K.S. Mazdiyasni, *J. Amer. Ceram. Soc.*, **80**, 903 (1997).
32. I.R. Gibson, G.P. Dransfield, and J.T.S. Irvine, *J. Eur. Ceram. Soc.*, **18**, 661 (1998).
33. J.E. Bauerle, *J. Phys. Chem. Solids*, **30**, 2657 (1969).
34. X.-D. Zhou, W. Huebner, I. Kosacki, and H.U. Anderson, *J. Amer. Ceram. Soc.*, **85**, 1757 (2002).
35. S. Dikmen, P. Shuk, M. Greenblatt, and H. Gocmez, *Solid State Sciences*, **4**, 585 (2002).
36. T.S. Zhang, P. Hing, H. Huang, and J.A. Kilner, *Solid State Ionics*, **148**, 567 (2002).
37. R.T. Dirstine, R.N. Blumenthal, and T.F. Kuech, *J. Electrochem. Soc.*, **126**, 264 (1979).
38. H. Arai, T. Kunisaki, Y. Shimizu, and T. Seiyama, *Solid State Ionics*, **20**, 241 (1986).
39. D. Perz-Coll, P. Nunez, J.R. Frade, and J.C.C. Abrantes, *Electrochimica Acta*, **48**, 1551 (2003).
40. Personal Communication between K. Rajender Reddy and J. Foreman, Nextech Materials, Inc.,USA.
41. T. He, Z. Lu, L. Pei, X. Huang, Z. Liu, and W. Su, *J. Alloys and Compounds*, **333**, 231 (2002).
42. M. Mogensen, N.M. Sammes, and G.A. Tompsett, *Solid State Ionics*, **129**, 63 (2000).
43. S. Kim and J. Maier, *J. Electrochem. Soc.*, **149**, J73 (2002).
44. M. Sahibzada, R.A. Rudkin, B.C.H. Steele, I.S. Metcalfe, and J.A. Kilner, *Solid Oxide Fuel Cells V- Electrochem. Soc. Proceed. Series* (1997), p. 244.